Journal of Mechanical Engineering, Science, and Innovation

e-ISSN: 2776-3536
2026, Vol. 6, No. 2
Page. 184-196
DOI: 10.31284/j.jmesi.2026.v6i2.9527
ejurnalitats.ac.id/jmesi

RESEARCH ARTICLE

Field Comparison of Vibration Before and After Structural Support Retrofit in a Variable-Speed Vertical Industrial Agitator

Aris Puja Widikda[1*], Widodo[2], Nugrahadi Djazaul Mukhsinin[1]

[1] Mechanical Technology Study Program, Politeknik Semen Indonesia, Gresik, Indonesia
[2] Mechanical Engineering Study Program, Politeknik Negeri Batam, Batam, Indonesia

Corresponding author:
Aris Puja Widikda
Mechanical Technology Study Program, Politeknik Semen Indonesia
Email: widikda@polteksi.ac.id
ORCID 0000-0003-0523-9777

ABSTRACT

Excessive vibration in vertically mounted industrial agitators can accelerate degradation of bearings, shafts, gearboxes, and supporting structures. This retrospective industrial study compares vibration measurements obtained before and after a structural support retrofit on a variable-speed vertical agitator used in a cement grinding-aid process. The two campaigns were conducted on different dates and with different vibration analysers; therefore, the observed differences are not interpreted as an isolated causal retrofit effect. At measurement point 1, horizontal vibration increased from 1.6 mm/s at 82 rpm to 13.0 mm/s at 203 rpm before the retrofit, whereas the post-retrofit campaign recorded 2.5 mm/s at 200 rpm, an observed before-and-after difference of 80.8%. At 50 Hz, points 2 and 3 changed from 6.2 to 1.7 mm/s and from 6.3 to 1.5 mm/s, respectively. Post-retrofit spectra and thermography are presented only as condition indicators; the largest reported looseness-related component was 0.84 m/s^2, and full-load motor temperature reached 66.3-67.7°C. The field evidence is associated with lower vibration levels following the support modification, while the dataset limitations preclude confirmation of resonance shifts or a uniquely causal mechanism.

Keywords: *Condition monitoring; Industrial agitator; Structural retrofit; Thermography; Vibration*

Received: September 11, 2026; Received in revised: October 21, 2026; Accepted: October 29, 2026
Handling Editor: Iftika Wardani

INTRODUCTION

Industrial agitators are essential rotating machines in chemical, mineral, cement, water-treatment, and other process industries because they provide continuous mixing, homogenisation, suspension, and mass-transfer functions. Their reliability depends on the combined dynamic behaviour of the electric motor, gearbox, shaft, impeller, bearings, mounting plate, and supporting structure. Vibration monitoring is widely used for rotating-machine condition assessment because changes in mechanical condition are reflected in vibration amplitude and frequency content [1], [2]. Reviews of induction-motor and rotating-machinery diagnostics also show that vibration signals remain central to identifying imbalance, misalignment, looseness, bearing faults, and other abnormalities, while electrical and thermal variables can provide complementary information [3], [4].

For a vertically mounted agitator, the support system is particularly important because the drive train forms a tall rotor-support assembly in which lateral excitation can be transmitted through the motor, gearbox, shaft, tank-top plate, and surrounding frame. Industrial evidence from a centrifuge-motor installation demonstrated that excessive vibration can originate from interaction between operating excitation and structural modes, with measured structural

Creative Commons CC BY-NC 4.0: This article is distributed under the terms of the Creative Commons Attribution 4.0 License (http://www.creativecommons.org/licenses/by-nc/4.0/). ©2026 The Author(s).

vibration reaching 10.65 mm/s against an alarm level of 7.1 mm/s [5]. Experimental rotor studies further show that changing support stiffness can alter critical-speed behaviour and reduce lateral vibration [6], while work on flexible vertical rotors reported that increasing pivot support stiffness reduced low-frequency whirl amplitude by about 51% and extended the stable operating-speed region [7]. These studies establish that support characteristics can materially influence the dynamic response of rotating systems.

Mixing equipment adds additional complexity because the shaft, bearings, sealing elements, and impeller operate as a coupled mechanical system. Recent work on vertical mixing-device shafts has shown that bearing elasticity and support conditions affect shaft stiffness and deflection, indicating that support behaviour should not be neglected in mechanical design [8]. Numerical and experimental investigations of rotor systems with supporting nonlinearity have similarly demonstrated that looseness and support-stiffness variations can generate complex speed-dependent responses [9], [10]. Pedestal-looseness studies have identified multiple harmonics, fractional-frequency components, and nonlinear responses as important diagnostic features [11]-[13]. Consequently, a reduction in overall vibration amplitude does not necessarily imply that all diagnostic spectral components have disappeared.

Frequency-domain interpretation therefore remains important after any mechanical corrective action. Contemporary reviews emphasize that rotating-machine faults can produce characteristic spectral and modulation patterns that are not fully represented by a single overall vibration value [14]. Infrared thermography also offers a non-contact complementary technique for observing thermal anomalies in rotating machinery [15]. In field practice, combining vibration magnitude, spectral content, temperature, rotational speed, and electrical loading can provide a more complete picture of equipment condition than relying on a single indicator [3], [15], [16].

Structural modifications are frequently applied in industry when high vibration is detected, but published studies often focus on numerical models, dedicated rotor test rigs, or modal-analysis campaigns. Research on bolted joints and rotating-part looseness has established how local stiffness variation affects rotor dynamics [17], [18], and nonlinear vibration-mitigation studies have demonstrated the sensitivity of rotating systems to support and fault interactions [19]. Structural optimisation has also been investigated for vibrating mixer mechanisms using finite-element and modal approaches [20]. However, comparatively fewer studies document a practical before-and-after support retrofit on an operating low-speed vertical industrial agitator at multiple speed settings, while also reporting residual spectral and thermal condition indicators.

Accordingly, this study presents a before-and-after field comparison of a structural support retrofit applied to a variable-speed vertical industrial agitator used in a cement grinding-aid process. The contribution is not the support concept itself, but the industrial evidence obtained across four operating-frequency settings, combined with point-specific vibration trends and post-retrofit spectral and thermographic condition indicators. The study asks how the horizontal vibration response changed between the two campaigns, whether the speed-sensitive response was spatially consistent, and what residual condition indicators remained after the support modification. Because the campaigns were conducted on different dates, used different analysers, and did not retain equivalent load documentation or repeated trials, the study is explicitly descriptive and does not claim an isolated causal treatment effect.

METHODS AND ANALYSIS

Industrial system and structural intervention

The investigated equipment was a vertically mounted motor-gearbox agitator installed at an Indonesian cement manufacturing facility. The main mixing tank had a nominal capacity of 2750 L, a documented working liquid volume of approximately 2000 L, a 1.3 m diameter, and a 2.1 m height; the tank shell was SS304 with a nominal plate thickness of 4 mm. The agitator shaft was SS304, 32 mm in diameter and approximately 2522 mm long, and the impeller comprised four SS304 blades, each approximately 4 mm thick, 80 mm wide, and 250 mm long. The drive used an Alliance Motori three-phase motor (type A-Y3A-100L2-4 B5), rated 3 kW, four-pole, 1420 rpm at 50 Hz, 220/380 V, 11.6/6.7 A, power factor 0.82, efficiency 82.6%, IP55, and insulation class F. The motor was coupled to an Alliance Motori AKAF-59-100B5 bevel-helical gear reducer, rated 3 kW with a nominal 7:1 ratio, 218 r/min specified output speed, and 600 N·m output torque. The nominal 1420 rpm motor speed divided by the 7:1 reduction gives approximately 203 rpm, which

is consistent with the 200-203 rpm field output speeds recorded at 50 Hz. Table 1 summarises the principal system and retrofit specifications.

Following the initial observation of excessive vibration at elevated speed, four inclined support members were installed around the motor-gearbox assembly and connected between 10 mm thick upper and lower plates. The supports were fabricated from stainless-steel pipe with a measured outer diameter of 50.8 mm and a wall thickness of 2 mm; the specific stainless-steel grade was not independently verified. Each member was installed at approximately 45° to the horizontal, with an approximate vertical separation and horizontal projection of 400 mm, a geometric span of approximately 566 mm, and an overall physical/cut length of approximately 575 mm. Pipe-to-plate joints were welded, while mechanical fastening with nuts was used at the designated attachment points. For an order-of-magnitude mechanical estimate, the hollow-pipe cross-sectional area is approximately 306.6 mm^2. Assuming a generic stainless-steel elastic-modulus range of 190-200 GPa solely for sensitivity analysis, the idealised axial stiffness of one 566 mm brace is approximately 103-108 kN/mm; its projected horizontal axial-stiffness component at 45° is approximately 51-54 kN/mm per engaged brace. These values are not the total machine-support stiffness because plate flexibility, weld compliance, bending, load sharing, and boundary conditions were not modelled. Consequently, the estimate supports only the qualitative expectation of increased structural restraint and is not used to infer a natural frequency or modal shift.

Table 1. Principal agitator-system and structural-retrofit specifications.

Component	Specification
Mixing tank	2750 L nominal capacity; approximately 2000 L working liquid volume; SS304 shell; 4 mm shell plate; diameter 1.3 m; height 2.1 m.
Motor	Alliance Motori A-Y3A-100L2-4 B5; 3 kW (4 HP); 4 pole; 1420 rpm at 50 Hz; 220/380 V; 11.6/6.7 A; cos φ 0.82; efficiency 82.6%; IP55; insulation class F; DE/NDE bearing 6206.
Gear reducer	Alliance Motori AKAF-59-100B5 bevel-helical reducer; 3 kW; nominal ratio 7:1; specified output speed 218 r/min; output torque 600 N·m.
Shaft and impeller	SS304 shaft, Ø32 mm × approximately 2522 mm; four SS304 blades, 4 mm thick × 80 mm wide × 250 mm long.
Support retrofit	Four inclined stainless-steel pipe members (grade not verified); measured OD 50.8 mm; wall thickness 2 mm; approximately 45° to horizontal; approximately 400 mm vertical separation; geometric span approximately 566 mm; overall physical/cut length approximately 575 mm.
Support connections	Upper and lower plates t = 10 mm; pipe-to-plate joints welded; mechanical fastening with nuts at designated attachment points.

Vibration measurements

The initial survey used a VIBXPERT II analyser (PRUFTECHNIK), whereas the post-retrofit survey used a Leonova Infinity analyser (SPM Instrument), as documented in the field records. The VIBXPERT II manufacturer data specify a dynamic vibration input capability up to 51.2 kHz, with acceleration measurement from 0.5 Hz [22]. The Leonova Infinity technical sheet for broadband ISO vibration specifies RMS velocity measurement over 10-1000 Hz and compatibility with SLD144 or IEPE-type vibration transducers [21]. In the present archive, both campaigns reported vibration velocity in mm/s at three corresponding positions. Direct comparison was restricted to the horizontal direction because that was the common direction retained in the pre-retrofit dataset. The exact sensor model, sensitivity, attachment method, calibration certificate, and measurement-band configuration used in either campaign were not retained, and no cross-instrument verification was performed. Therefore, the two measurement chains cannot be treated as metrologically equivalent, and the numerical comparison is interpreted only as an observed industrial before-and-after field difference. Table 2 summarises the documented differences between the campaigns.

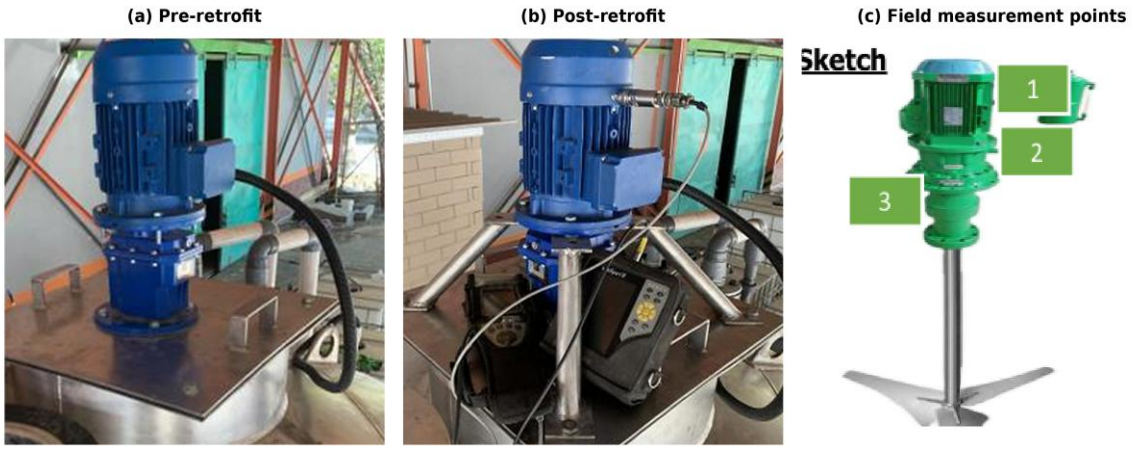


Figure 1. Field configuration and measurement arrangement: (a) pre-retrofit condition without additional support; (b) post-retrofit condition with inclined support members; and (c) field measurement points.

The post-retrofit spectral report contained instrument-generated diagnostic components at bearing positions No. 1, No. 2, and No. 3, categorised as looseness (3rd-10th harmonics and 0.5-3.5 harmonics), unbalance, misalignment, and vane/impeller-related responses. The retained plots covered 0-1000 Hz. These categories are treated as instrument-generated condition indicators rather than definitive fault confirmation because no controlled fault validation, bearing-defect-frequency calculation, or disassembly inspection was performed. The archived plots also do not retain sufficiently precise peak-cursor data or a synchronised shaft-speed record for the spectral acquisition time; therefore, exact peak orders relative to shaft speed, gear-mesh frequency, vane-passing frequency, or structural modes cannot be reconstructed. No pre-retrofit spectrum was retained, so the post-retrofit spectra are used solely to describe the residual machine condition and not to quantify a spectral effect of the retrofit.

Thermographic assessment

Infrared thermography was available only for the post-retrofit condition. The retained field records used an emissivity setting of 0.95 for the motor, gearbox, and shaft images and a reflected-temperature setting of 34.0°C. Ambient air temperature was not independently recorded and is therefore not inferred from the reflected-temperature setting. After the documented 30 min half-load run, maximum temperatures were 57.2°C for the motor, 44.1°C for the gearbox, and 33.1°C for the shaft. During full-load operation, the first motor image recorded 67.7°C, the gearbox image recorded 48.2°C, and a second motor image obtained approximately two minutes later recorded 66.3°C. These measurements are interpreted only as post-retrofit thermal condition indicators because no equivalent pre-retrofit thermographic baseline exists.

Comparative analysis and data-quality constraints

Before-and-after comparison was performed point by point at the same inverter-frequency settings. The corresponding rotational speeds differed by only 1-3 rpm between campaigns, allowing descriptive comparison at nominally matched speed settings. For each measurement point, the observed before-and-after difference was calculated using Eq. (1), where Vpre is the pre-retrofit horizontal vibration velocity and Vpost is the corresponding post-retrofit value. Each archived operating condition is represented by a single retained field reading; repeated trials, time-series records, and an additional independent operating campaign were not available. Accordingly, no inferential statistical test, repeatability statistic, confidence interval, or causal treatment-effect estimate is reported.

$$R_v = ((Vpre - Vpost) / Vpre) \times 100\% \quad (1)$$

The field records report vibration velocity to a resolution of 0.1 mm/s. A half-digit reporting-resolution bound of ±0.05 mm/s can therefore be quantified from the retained values, but this is not a calibrated measurement uncertainty. For the headline comparison of 13.0 mm/s and 2.5 mm/s, a rounding-only sensitivity check gives an observed difference range equivalent to

approximately 80.3-81.2%. This check excludes analyser accuracy, sensor sensitivity, mounting, bandwidth, calibration, process-load variability, and date-to-date operating differences. Because these components cannot be reconstructed from the archive, a traceable uncertainty budget is not claimed.

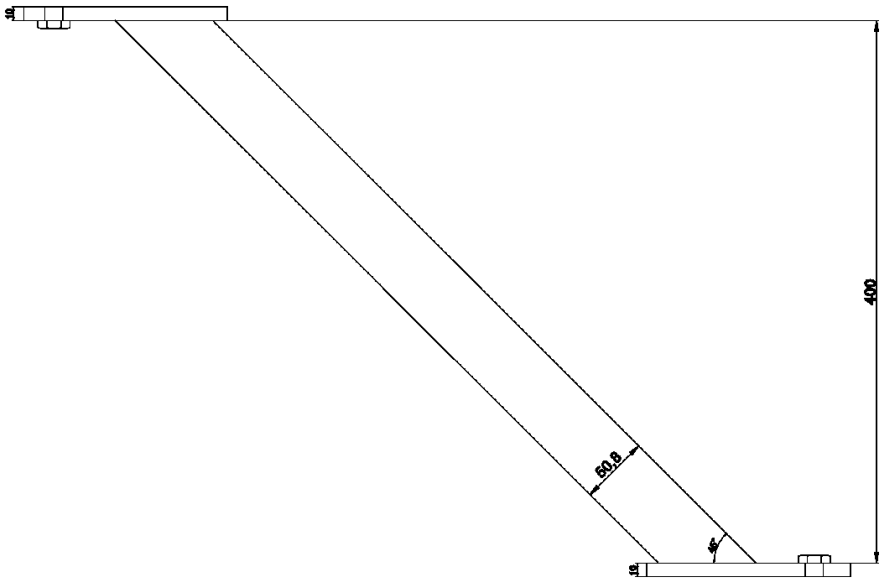


Figure 2. Dimensioned side-view schematic of one inclined support member. Four identical members were installed around the motor-gearbox assembly; pipe, plate, and connection specifications are summarised in Table 1.

Table 2. Comparison of the pre- and post-retrofit industrial field measurement campaigns.

Parameter	Pre-retrofit trial	Post-retrofit trial
Date	8 August 2025	27 August 2025
Additional structural support	Absent	Installed
Inverter frequency	20, 30, 40, 50 Hz	20, 30, 40, 50 Hz
Output speed	82, 122, 163, 203 rpm	81, 120, 161, 200 rpm
Vibration analyser	VIBXPERT II (PRUFTECHNIK)	Leonova Infinity (SPM Instrument)
Primary comparative direction	Horizontal velocity	Horizontal velocity
Loading documentation	Not specified with equivalent detail in the surviving 8 August field sheet	Load and no-load conditions explicitly documented
Spectrum information	Not retained in initial sheet	Available at three bearing positions
Thermography	Not available	Half-load and full-load available
Measured quantity used for direct comparison	Horizontal vibration velocity, mm/s	Horizontal vibration velocity, mm/s
Published / retained frequency information	VIBXPERT II dynamic input capability up to 51.2 kHz; acceleration from 0.5 Hz [22]	Leonova Infinity ISO vibration velocity: 10-1000 Hz; retained FFT plots span 0-1000 Hz [21]
Sensor model and sensitivity	Not retained in field archive	Not retained in field archive
Sensor mounting method	Not retained	Not retained
Calibration certificate / traceability	Not retained	Not retained
Cross-instrument verification	Not performed / not retained	Not performed / not retained
Spectrum baseline	Not retained	Available only post-retrofit

RESULTS AND DISCUSSIONS

Speed-dependent vibration before and after retrofit

The pre-retrofit field trial showed a pronounced speed-dependent increase in horizontal vibration. At 20 Hz (82 rpm), points 1-3 measured 1.6, 0.8, and 0.8 mm/s. At 30 Hz (122 rpm), the values increased to 5.0, 2.4, and 2.0 mm/s; at 40 Hz (163 rpm), to 10.5, 4.7, and 2.8 mm/s; and at 50 Hz (203 rpm), to 13.0, 6.2, and 6.3 mm/s. The strongest response occurred at point 1, particularly at the two highest speeds.

In the 27 August post-retrofit load trial, horizontal vibration values were lower at all three positions than the corresponding values retained from the 8 August campaign. At 20 Hz (81 rpm), points 1-3 measured 0.2, 0.1, and 0.1 mm/s; at 30 Hz (120 rpm), 1.3, 0.4, and 0.3 mm/s; at 40 Hz (161 rpm), 2.2, 0.6, and 0.7 mm/s; and at 50 Hz (200 rpm), 2.5, 1.7, and 1.5 mm/s. Figure 3 presents the point-specific speed-vibration response, while Table 3 provides the paired numerical comparison. Because the campaigns differed in analyser and load documentation, these values are compared descriptively rather than interpreted as a controlled treatment effect.

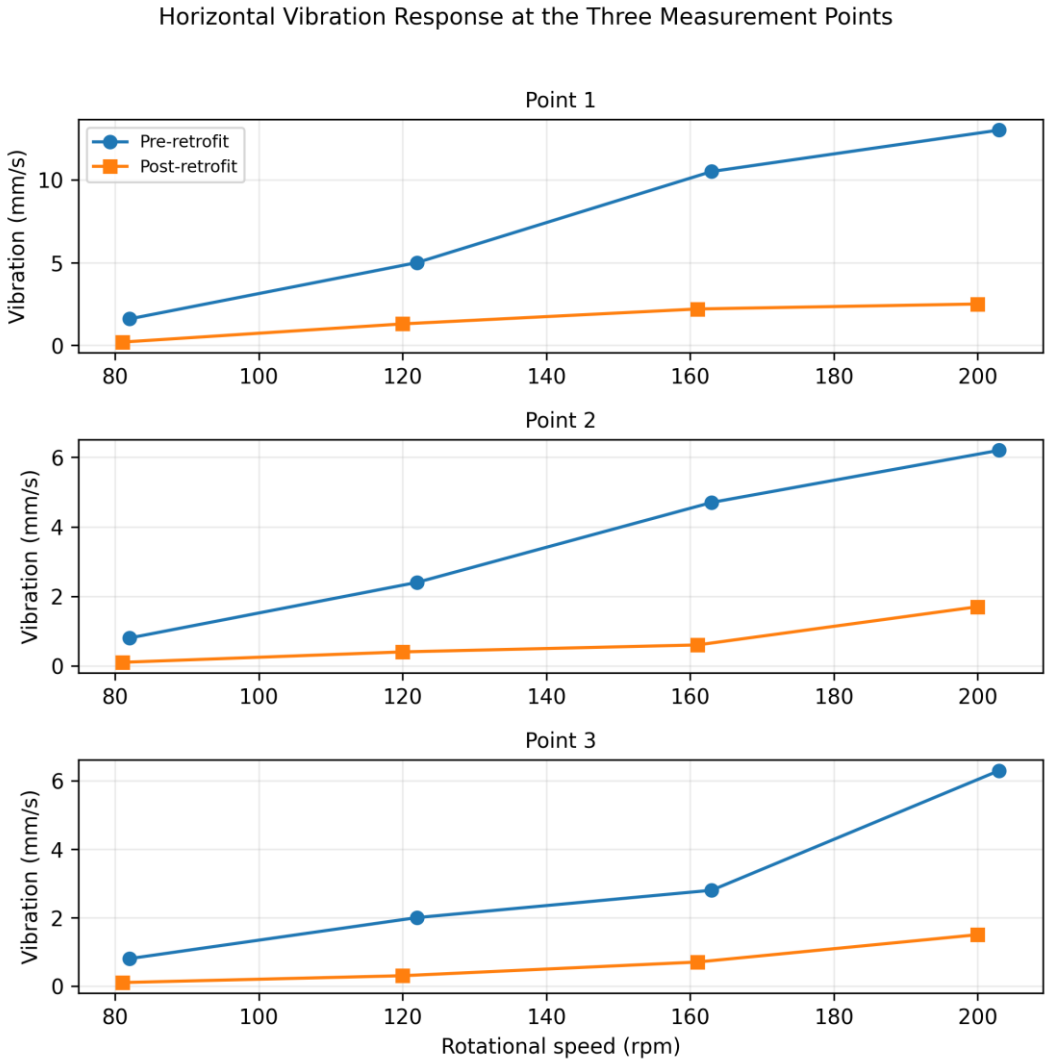


Figure 3. Point-specific horizontal vibration response versus rotational speed in the pre- and post-retrofit field campaigns.

Point 1, which exhibited the largest absolute vibration amplitudes, also showed a strong monotonic speed dependence. Before the retrofit, Point 1 horizontal vibration increased from 1.6 to 5.0, 10.5, and 13.0 mm/s at 82, 122, 163, and 203 rpm, respectively; the corresponding 1X rotational frequencies were approximately 1.37, 2.03, 2.72, and 3.38 Hz. Because only four discrete speed points were retained and no phase, run-up/coast-down, bump-test, operational-modal, or natural-frequency measurements were available, this monotonic increase does not

resolve a resonance peak or identify a critical speed. The post-retrofit Point 1 values remained speed dependent (0.2, 1.3, 2.2, and 2.5 mm/s at 81, 120, 161, and 200 rpm) but at substantially lower absolute amplitude. Point 3 showed an additional marked increase at the upper end of the speed range: before the retrofit, horizontal vibration increased from 2.8 mm/s at 163 rpm to 6.3 mm/s at 203 rpm, a 125% vibration increase for a 24.5% speed increase. A similar speed-sensitive trend remained in the post-retrofit campaign, where Point 3 increased from 0.7 mm/s at 161 rpm to 1.5 mm/s at 200 rpm. Accordingly, the field evidence supports lower response amplitude in the later campaign, but it does not demonstrate elimination of resonance, identification of a critical speed, or a shift in natural frequency.

Table 3. Point-specific horizontal vibration before and after retrofit and observed before-and-after difference.

Freq.	Speed pre/post	Point 1: pre→post	Point 2: pre→post	Point 3: pre→post
20 Hz	82/81 rpm	1.6→0.2 (87.5%)	0.8→0.1 (87.5%)	0.8→0.1 (87.5%)
30 Hz	122/120 rpm	5.0→1.3 (74.0%)	2.4→0.4 (83.3%)	2.0→0.3 (85.0%)
40 Hz	163/161 rpm	10.5→2.2 (79.0%)	4.7→0.6 (87.2%)	2.8→0.7 (75.0%)
50 Hz	203/200 rpm	13.0→2.5 (80.8%)	6.2→1.7 (72.6%)	6.3→1.5 (76.2%)

Observed vibration reduction and structural interpretation

Across all twelve point-frequency pairs, the observed before-and-after difference ranged from 72.6% to 87.5% (Figure 4). At point 1, the calculated differences were 87.5%, 74.0%, 79.0%, and 80.8% at 20, 30, 40, and 50 Hz, respectively. At the highest operating setting, points 2 and 3 changed by 72.6% and 76.2%, respectively. The lower values in the later campaign occurred at all monitored positions and speed settings; however, because instrumentation and operating-condition documentation were not equivalent, the percentage values are descriptive field differences rather than isolated estimates of retrofit effectiveness.

The lower post-retrofit response is mechanically consistent with the addition of inclined structural restraint. The support geometry provides an idealised axial load path between the upper and lower plates. Using the measured pipe geometry (OD 50.8 mm, wall 2 mm, geometric span approximately 566 mm) gives a cross-sectional area of approximately 306.6 mm^2. A sensitivity estimate using E = 190-200 GPa gives an idealised axial stiffness of approximately 103-108 kN/mm for one brace and a 45° horizontal axial-stiffness component of approximately 51-54 kN/mm per engaged brace. This is not the total lateral stiffness of the machine-support assembly and neglects weld and plate compliance, member bending, load sharing, tank-top flexibility, and boundary conditions. The estimate therefore provides only an order-of-magnitude explanation for increased restraint; it does not demonstrate a change in damping, natural frequency, or modal shape [5]-[8].

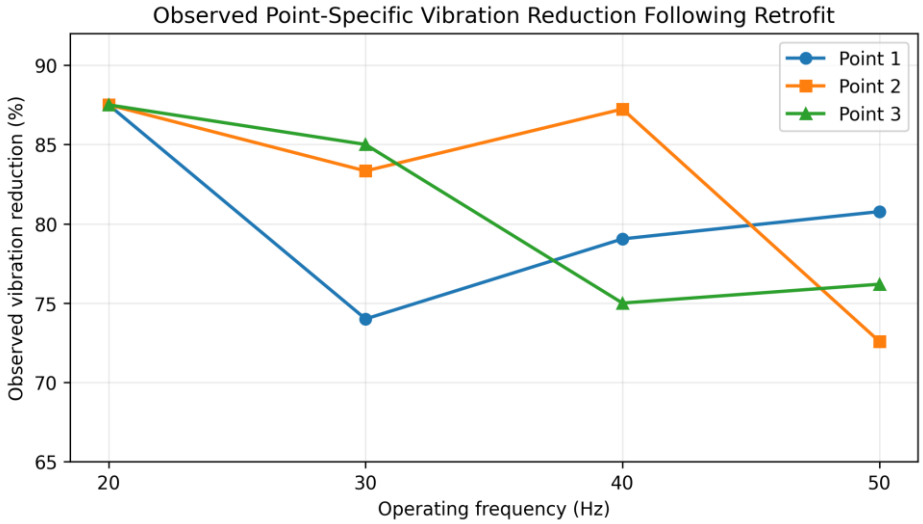
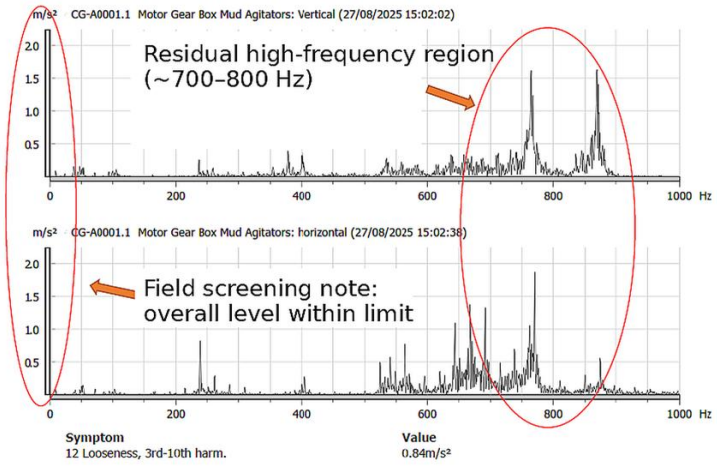
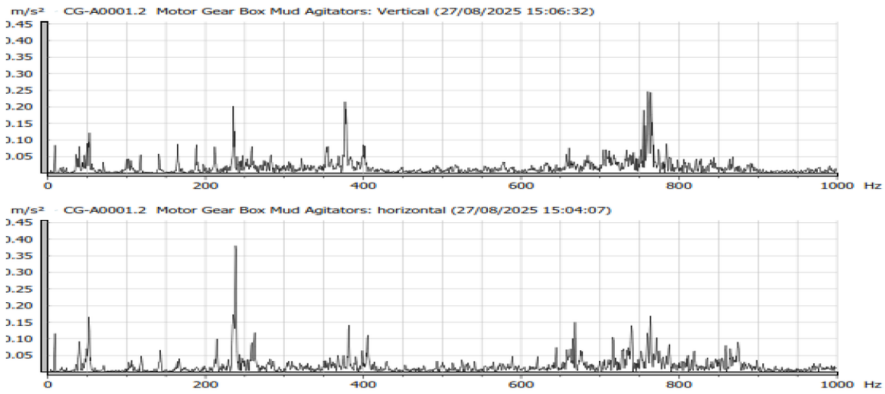


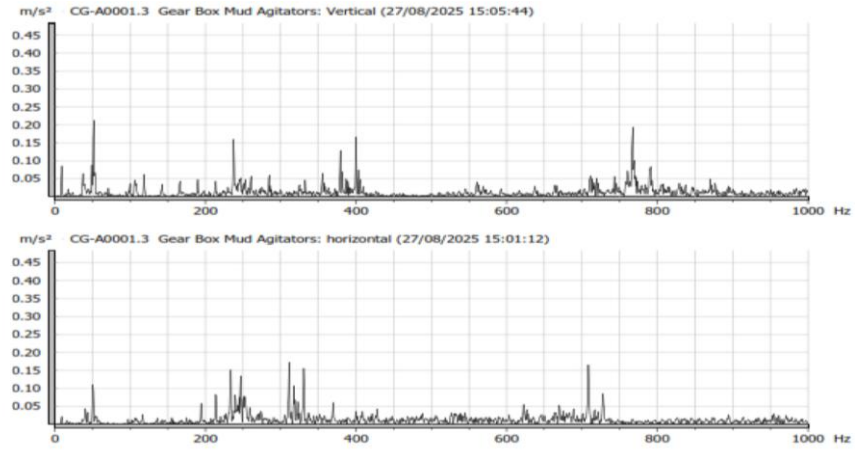
Figure 4. Observed point-specific before-and-after vibration differences between the two field campaigns.



(a). Bearing position No.1



(b). Bearing position No.2



(b). Bearing position No.3

Figure 5. Post-retrofit vibration spectra at bearing positions No. 1-No. 3; diagnostic labels are those reported by the field analyser.

Spatial distribution of vibration

The vibration response was not spatially uniform. At the highest pre-retrofit speed of 203 rpm, point 1 reached 13.0 mm/s, while points 2 and 3 were 6.2 and 6.3 mm/s. After retrofit at 200 rpm, the corresponding values were 2.5, 1.7, and 1.5 mm/s. Thus, point 1 remained the location of the largest measured response even after the overall reduction. This persistent spatial pattern identifies point 1 as the most informative location for subsequent condition monitoring of the drive assembly.

The original maintenance sheets classified vibration using an ISO 10816 Class III rigid-machine screening table, in which 0.1-1.8 mm/s was labelled good, 1.9-4.5 mm/s acceptable, 4.6-

11.0 mm/s tolerable, and values above 11.0 mm/s bad. In that historical plant protocol, the 13.0 mm/s pre-retrofit value at Point 1 exceeded the highest screening threshold, whereas the 2.5 mm/s post-retrofit value lay within the plant-labelled acceptable range. These bands are not adopted here as a formal acceptance criterion for the investigated agitator. The motor is rated only 3 kW, whereas ISO 20816-3:2022 specifies general evaluation requirements for industrial machinery above 15 kW [23]. Therefore, the study reports the plant classification only as historical maintenance context and does not claim formal compliance with a current ISO acceptance zone or a manufacturer-specific vibration limit.

Post-retrofit spectral indicators

Post-retrofit spectra at the three bearing positions are shown in Figure 5, and the instrument-reported diagnostic indicators are summarised in Table 4. Bearing position No. 1 had the largest 3rd-10th harmonic component categorised by the analyser as looseness, at 0.84 m/s^2, compared with 0.40 m/s^2 at bearing No. 2 and 0.03 m/s^2 at bearing No. 3. Bearing No. 1 also showed a vane/impeller-related indicator of 0.13 m/s^2 and a distinct high-frequency region around 700-800 Hz in the retained plot. However, exact peak cursor frequencies and a synchronised shaft-speed record were not retained for the spectral capture, so these peaks cannot be assigned quantitatively to shaft orders, gear-mesh frequency, vane-passing frequency, or structural resonance. The original field annotation associated the 700-800 Hz region with loading on the vertically oriented motor bearing, but the present study treats that statement only as the field diagnosis and not as a validated mechanism.

Table 4. Instrument-reported post-retrofit spectral diagnostic indicators. NR = not reported.

Indicator	Bearing No. 1	Bearing No. 2	Bearing No. 3
Looseness, 3rd-10th harmonic	0.84 m/s^2	0.40 m/s^2	0.03 m/s^2
Looseness, 0.5-3.5 harmonic	0.01 m/s^2	0.03 m/s^2	0.01 m/s^2
Unbalance	0.02 m/s^2	0.01 m/s^2	0.02 m/s^2
Misalignment	NR	0.05 m/s^2	0.02 m/s^2
Vane and impeller	0.13 m/s^2	0.01 m/s^2	0.02 m/s^2

Studies of pedestal and joint looseness show that local support changes can generate harmonics, fractional-frequency content, and nonlinear response [9]-[13]. Nevertheless, the present post-retrofit symptom values cannot establish whether looseness-related components decreased, remained unchanged, or were introduced after the modification because no pre-retrofit spectrum was retained. The spectral section is therefore restricted to residual post-retrofit condition assessment. Future work would require synchronised rpm, raw spectral cursor data, and a pre/post spectrum obtained with the same transducer and analyser configuration to support order-based diagnosis.

Post-retrofit thermal condition

Figure 6 presents the post-retrofit half-load thermography. Maximum temperatures were 57.2°C for the motor, 44.1°C for the gearbox, and 33.1°C for the shaft, producing a clear component-level temperature gradient. Under full load (Figure 7), the gearbox reached 48.2°C, while two motor captures recorded maxima of 67.7°C and 66.3°C. The two full-load motor maxima differed by 1.4°C over the short measurement interval. Relative to the half-load motor maximum, the two full-load captures were 10.5°C and 9.1°C higher, respectively; the gearbox increased by 4.1°C from half to full load. The field report also recorded approximately 6 A at 50 Hz and labelled this condition as overload. However, the retained motor specification gives a rated current of 6.7 A at 380 V (11.6 A at 220 V). Without a retained line-voltage record and full electrical operating data, the present study does not independently classify the approximately 6 A measurement as an electrical overload.

The thermal data do not establish a thermal effect of the structural support because no pre-retrofit thermographic baseline exists. Instead, they characterise the post-retrofit thermal condition and show that lower vibration in the later campaign did not eliminate thermal loading as process load increased. This supports the use of vibration, frequency-domain information, temperature, current, rotational speed, and process condition as complementary indicators rather than relying on a single overall vibration value [1], [15], [16].

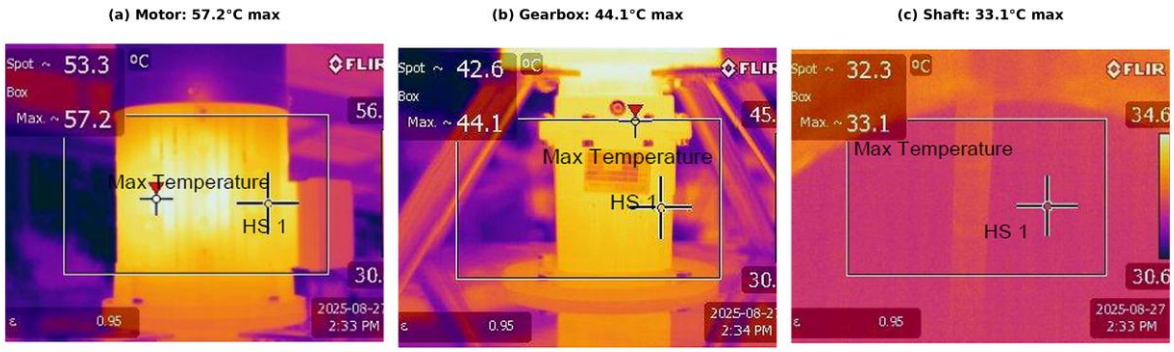


Figure 6. Post-retrofit thermography under half-load operation: (a) motor, (b) gearbox, and (c) agitator shaft.

Practical implications and limitations

For industrial practice, this case does not imply that structural reinforcement is a generic remedy for excessive agitator vibration. A support retrofit is most defensible when vibration increases strongly with operating speed, is spatially concentrated near the drive-support region, and conventional sources have first been investigated. A practical diagnostic sequence is therefore: (1) verify speed, process load, liquid level, and repeatability; (2) inspect imbalance, alignment, bearings, looseness, gearbox excitation, shaft condition, and impeller/process-induced forcing using appropriate spectral and mechanical checks; (3) evaluate structural flexibility using multi-point vibration, phase, run-up/coast-down, bump testing, operational modal analysis, or finite-element analysis where feasible; and (4) consider structural reinforcement only when the evidence supports inadequate restraint or structural amplification. After any modification, the response should be verified at multiple points and complemented by spectral, thermal, and electrical monitoring. In the present case, Point 1 remained the highest-vibration monitoring location after the modification and should remain a priority for subsequent condition monitoring.

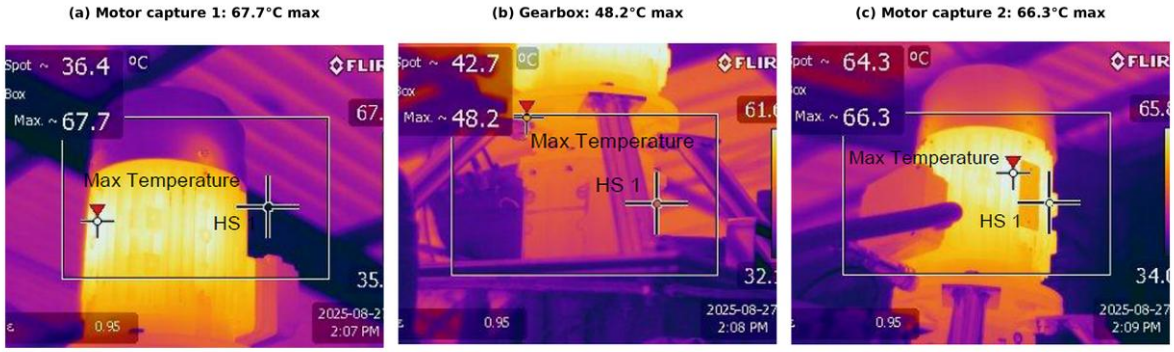


Figure 7. Post-retrofit thermography under full-load operation: (a) first motor capture, (b) gearbox, and (c) second motor capture.

Several limitations are intrinsic to the retrospective industrial dataset. First, each operating point is represented by a single retained field reading rather than repeated controlled trials, so reproducibility, process variability, and statistical significance cannot be quantified. Second, the loading condition of the 8 August campaign was not documented with the same detail as the 27 August load trial. Third, different vibration analysers were used, and the retained archive does not include the exact sensor model, mounting method, sensitivity, calibration certificate, bandwidth setting, or cross-instrument verification needed for a traceable uncertainty budget. Fourth, no pre-retrofit spectrum was retained. Fifth, no phase, run-up/coast-down, bump-test, operational-modal, structural-stiffness, damping, or natural-frequency measurements were available, so resonance and modal-frequency shifts cannot be confirmed. Finally, thermography was available only after the retrofit, ambient air temperature was not independently recorded, and the stainless-steel support grade was not verified. These constraints mean that the observed 72.6-87.5% differences cannot be attributed exclusively to the structural support retrofit; the

study should be interpreted as a documented industrial before-and-after case comparison that motivates more controlled validation.

Table 5. Maximum temperatures recorded during the post-retrofit thermographic assessment.

Operating condition	Component / capture	Maximum temperature
Half load	Motor	57.2°C
Half load	Gearbox	44.1°C
Half load	Shaft	33.1°C
Full load	Motor - capture 1	67.7°C
Full load	Gearbox	48.2°C
Full load	Motor - capture 2	66.3°C

CONCLUSIONS

This industrial before-and-after field comparison documented substantially lower horizontal vibration values in the later campaign following installation of four inclined structural supports. At Point 1, the highest comparable-speed value changed from 13.0 mm/s at 203 rpm to 2.5 mm/s at 200 rpm, an observed difference of 80.8%; at the same 50 Hz setting, Points 2 and 3 changed from 6.2 to 1.7 mm/s and from 6.3 to 1.5 mm/s. Across all point-frequency pairs, the descriptive differences ranged from 72.6% to 87.5%. Point 1 remained strongly speed dependent in both campaigns, and Point 3 retained a marked upper-speed increase; therefore, the dataset supports lower response amplitude in the later campaign but does not identify a critical speed or demonstrate elimination or displacement of resonance. Post-retrofit spectral indicators remained largest at Bearing No. 1, with an analyser-reported 3rd-10th harmonic looseness-related value of 0.84 m/s^2, while full-load motor thermography recorded 66.3-67.7°C. Because the campaigns used different analysers, the initial load condition was incompletely documented, and no repeated or modal measurements were retained, these differences cannot be attributed exclusively to the retrofit. The general engineering implication is that structural support condition should be considered as one element of a multi-parameter diagnostic process rather than as a universal corrective action.

ACKNOWLEDGEMENTS

The authors acknowledge the reliability-maintenance personnel and plant team of PT Semen Indonesia (Persero) Tbk. for supporting the field trials, vibration measurements, and thermographic inspection.

DECLARATION OF CONFLICTING INTERESTS

The authors declare that there are no potential conflicts of interest regarding the research, authorship, and/or publication of this article.

FUNDING

The authors report that no specific research funding was received for this study.

AUTHOR CONTRIBUTIONS

Aris Puja Widikda: conceptualisation, methodology, investigation, formal analysis, visualisation, writing - original draft, and writing - review and editing. Widodo and Nugrahadi Djazaul Mukhsinin: manuscript review and final approval. All authors reviewed and approved the final manuscript.

USE OF GENERATIVE AI

During the preparation of this work, ChatGPT (OpenAI, GPT-5.6 Sol) was used to assist with manuscript structuring, English-language refinement, and data visualisation. The authors reviewed and edited the output and take full responsibility for the content of the published article.

DATA AVAILABILITY

The data supporting the findings of this study are available from the corresponding author on reasonable request, subject to applicable industrial confidentiality, permission, and data-sharing requirements.

REFERENCES

[1] M. Tiboni, C. Remino, R. Bussola, and C. Amici, "A review on vibration-based condition monitoring of rotating machinery," Applied Sciences, vol. 12, no. 3, Art. no. 972, 2022, doi: 10.3390/app12030972.
[2] M. H. Mohd Ghazali and W. Rahiman, "Vibration analysis for machine monitoring and diagnosis: A systematic review," Shock and Vibration, vol. 2021, Art. no. 9469318, 2021, doi: 10.1155/2021/9469318.
[3] P. Gangsar and R. Tiwari, "Signal based condition monitoring techniques for fault detection and diagnosis of induction motors: A state-of-the-art review," Mechanical Systems and Signal Processing, vol. 144, Art. no. 106908, 2020, doi: 10.1016/j.ymssp.2020.106908.
[4] J. Chen, C. Lin, D. Peng, and H. Ge, "Fault diagnosis of rotating machinery: A review and bibliometric analysis," IEEE Access, vol. 8, pp. 224985-225003, 2020, doi: 10.1109/ACCESS.2020.3043743.
[5] A. K. Devaraj and R. Adhikari, "Vibration analysis of the base structure supporting a centrifuge-motor assembly in a petroleum oil refinery," Journal of The Institution of Engineers (India): Series C, vol. 104, pp. 393-401, 2023, doi: 10.1007/s40032-023-00919-y.
[6] S. Laine, S. Haikonen, T. Tiainen, and R. Viitala, "Rotor resonance avoidance by continuous adjustment of support stiffness," International Journal of Mechanical Sciences, vol. 270, Art. no. 109092, 2024, doi: 10.1016/j.ijmecsci.2024.109092.
[7] Q. Liu, C. Tang, T. Wu, and Y. Bai, "Influence of pivot support stiffness on dynamic characteristics of vertical rotor system," Journal of Vibroengineering, vol. 25, no. 6, pp. 1040-1052, 2023, doi: 10.21595/jve.2023.23136.
[8] L. Bibire, A.-D. Chitimus, and V. Ciubotariu, "Design of mixing device shafts based on a proposed calculation method supported by finite element method analysis," Machines, vol. 12, no. 7, Art. no. 479, 2024, doi: 10.3390/machines12070479.
[9] H. Zhang, K. Lu, W. Zhang, and C. Fu, "Investigation on dynamic behaviors of rotor system with looseness and nonlinear supporting," Mechanical Systems and Signal Processing, vol. 166, Art. no. 108400, 2022, doi: 10.1016/j.ymssp.2021.108400.
[10] J. Lin, Y. Zhao, P. Wang, Y. Wang, Q. Han, and H. Ma, "Nonlinear responses of a rotor-bearing-seal system with pedestal looseness," Shock and Vibration, vol. 2021, Art. no. 9937700, 2021, doi: 10.1155/2021/9937700.
[11] M. Jiang, J. Wu, X. Peng, and X. Li, "Nonlinearity measure based assessment method for pedestal looseness of bearing-rotor systems," Journal of Sound and Vibration, vol. 411, pp. 232-246, 2017, doi: 10.1016/j.jsv.2017.09.002.
[12] Z. Qin, Q. Han, and F. Chu, "Bolt loosening at rotating joint interface and its influence on rotor dynamics," Engineering Failure Analysis, vol. 59, pp. 456-466, 2016, doi: 10.1016/j.engfailanal.2015.11.002.
[13] S. Wei, W. Lu, and F. Chu, "Speed characteristics of disk-shaft system with rotating part looseness," Journal of Sound and Vibration, vol. 469, Art. no. 115127, 2020, doi: 10.1016/j.jsv.2019.115127.
[14] P. Zhou, S. Chen, Q. He, D. Wang, and Z. Peng, "Rotating machinery fault-induced vibration signal modulation effects: A review with mechanisms, extraction methods and applications for diagnosis," Mechanical Systems and Signal Processing, vol. 200, Art. no. 110489, 2023, doi: 10.1016/j.ymssp.2023.110489.
[15] R. Wang, X. Zhan, H. Bai, E. Dong, Z. Cheng, and X. Jia, "A review of fault diagnosis methods for rotating machinery using infrared thermography," Micromachines, vol. 13, no. 10, Art. no. 1644, 2022, doi: 10.3390/mi13101644.
[16] C. Mongia, D. Goyal, and S. Sehgal, "Vibration response-based condition monitoring and fault diagnosis of rotary machinery," Materials Today: Proceedings, vol. 50, pt. 5, pp. 679-683, 2022, doi: 10.1016/j.matpr.2021.04.395.
[17] Y. Yang, H. Ouyang, Y. Yang, D. Cao, and K. Wang, "Vibration analysis of a dual-rotor-bearing-double casing system with pedestal looseness and multi-stage turbine blade-casing rub," Mechanical Systems and Signal Processing, vol. 143, Art. no. 106845, 2020, doi: 10.1016/j.ymssp.2020.106845.
[18] Y. Yang, G. Chen, H. Ouyang, Y. Yang, and D. Cao, "Nonlinear vibration mitigation of a rotor-casing system subjected to imbalance-looseness-rub coupled fault," International Journal of Non-Linear Mechanics, vol. 122, Art. no. 103467, 2020, doi: 10.1016/j.ijnonlinmec.2020.103467.
[19] Y. Liu, Y. Zhao, J. Li, H. Lu, and H. Ma, "Feature extraction method based on NOFRFs and its application in faulty rotor system with slight misalignment," Nonlinear Dynamics, vol. 99, pp. 1763-1777, 2020, doi: 10.1007/s11071-019-05340-8.

[20] W. Zhao, C. Yue, and W. Shen, "Finite element simulation and structure optimization of the agitating mechanism of double shaft vibrating mixer," Journal of Mechanical Strength, vol. 42, no. 6, pp. 1496-1502, 2020, doi: 10.16579/j.issn.1001.9669.2020.06.032.

[21] SPM Instrument AB, "Leonova Infinity – Vibration ISO 2372," Technical Data TD-225 B, Strängnäs, Sweden. [Online]. Available: https://extranet.spminstrument.se/Documents/Downloads/Support/TD-Sheets/LEOInB.pdf. [Accessed: 21-Oct-2026].

[22] PRUFTECHNIK, "VIBXPERT II Technical Data," Fluke Deutschland GmbH, Ismaning, Germany. [Online]. Available: https://www.pruftechnik.com/fileadmin/Products-Services/Products/Condition-Monitoring-Systems/Vibration-Analysis-and-Balancing/VIBXPERT-II/Downloads/6013867b_en_fds_3419_vibxpert_ii_ds.pdf. [Accessed: 21-Oct-2026].

[23] International Organization for Standardization, ISO 20816-3:2022, Mechanical vibration — Measurement and evaluation of machine vibration — Part 3: Industrial machinery with a power rating above 15 kW and operating speeds between 120 r/min and 30 000 r/min. Geneva, Switzerland: ISO, 2022.